NASA CONTRACTOR REPORT

NASA CR-442

NASA CR-442

A THEORETICAL ANALYSIS OF TUBE FRAGMENTATION

by D. P. Updike

Prepared under Grant No. NsG-488 *by*
BROWN UNIVERSITY
Providence, R. I.
for

NATIONAL AERONAUTICS AND SPACE ADMINISTRATION • WASHINGTON, D. C. • APRIL 1966

NASA CR-442

A THEORETICAL ANALYSIS OF TUBE FRAGMENTATION

By D. P. Updike

Prepared under Grant No. NsG-488 by
BROWN UNIVERSITY
Providence, R.I.

for

NATIONAL AERONAUTICS AND SPACE ADMINISTRATION

For sale by the Clearinghouse for Federal Scientific and Technical Information
Springfield, Virginia 22151 – Price $0.75

Summary

This paper develops a theoretical analysis to determine the force level attained in a cylindrical metal tube when the tube is fragmenting or splitting and rolling on a rigid die. The tube is treated as a thin, rigid-perfectly plastic cylindrical shell which fractures when a critical level of maximum strain is attained. The die has a semi-toroidal shape in order to expand the tube radially and to bend it meridianally, thus leading to fragmentation, i.e., fractures running in two perpendicular directions. It is shown that in the fragmentation regime the meridianally running cracks advance rapidly at first and then may become arrested. It is also shown that localized high bending strains develop and lead to transverse fracture. The energy absorbed during the process is evaluated through a numerical procedure which considers successive configurations of the deforming tube. The effect of contact friction on the energy absorbed is considered and found to be significant.

Nomenclature

The tube mean radius and thickness are A and T, respectively. All dimensionless length parameters are normalized with respect to the shell parameter $\sqrt{AT}$.

a	$A/\sqrt{AT}$, dimensionless tube mean radius
b	see eq. (25)
D	dimensionless displacement of the tube
f	see eq. (12)
F	die contact force per unit circumference
g	ξ - coordinate of the plastic hinge
h	dimensionless tube half thickness
H(s)	Heaviside unit step function of s
ℓ	dimensionless petal length,
ℓ^*	lower limit of integrals, see eq. (15)
m	$M/\sigma_o T^2$, dimensionless bending moment
M	bending moment per unit length
n_x	$N_x/\sigma_o T$, dimensionless meridianal force
N_x	meridianal force per unit length
n_θ	$N_\theta/\sigma_o T$, dimensionless circumferential force
N_θ	circumferential force per unit length
p	dimensionless length of plastic region,
$\bar{p}$	contact pressure
q	$Q\sqrt{AT}/\sigma_o T^2$, dimensionless shearing force
Q	shearing force per unit length
R	dimensionless die radius
R_1	dimensionless modified die radius
t	$2h = T/\sqrt{AT}$, dimensionless tube thickness
u	dimensionless radial displacement of middle surface
u'	dimensionless radial displacement of inner surface
v	dimensionless radial velocity
V	radial velocity
w	$\frac{dD}{d\tau}$, dimensionless tube axial velocity
x	dimensional position coordinate
y	dimensionless length projection on tube axis
z	dimensionless projection of petal on tube axis
$\delta(s)$	Dirac delta function of s

ε	average circumferential strain
$\dot{\varepsilon}$	circumferential strain rate
η	$x/\sqrt{AT}$, dimensionless position coordinate measured from the plastic hinge in the shell
$\varkappa$	dimensionless curvature
$\dot{\varkappa}$	dimensionless curvature rate
$\dot{K}$	dimensional curvature rate
$\lambda, \lambda', \Lambda$	arbitrary positive multipliers
μ	friction coefficient
ν	angle, see eq. (26)
ξ	dimensionless position coordinate measured from the petal tip
σ, σ'	compressive stress in the undeformed portion of the tube. Prime indicates that the effect of axial force on the yield surface has been considered.
σ_o	material flow stress in tension or compression
τ	dimensionless time parameter
φ	slope angle
Φ	function defining flow surface
ψ	die angle
ω	dimensionless angular velocity

Subscripts

c	refer to location at crack tip or petal root
h	refer to location at plastic hinge
t	refer to location at petal tip
o	initial condition, except for σ_o

Introduction

A method proposed for the absorption of kinetic energy is the process of fragmentation of metal tubing. A metal circular tube is forced over a die causing circumferential expansion and meridianal bending of the tube as shown in figures 1 (a) and 1(b). Due to the limited ductility of the material, cracks develop along meridianal lines so that a number of petals are formed at the end of the tube. In the fragmenting regime these petals grow and then break off due to the large bending strains developed. The petal growth and breaking process then repeats. After a few petals have broken off, the process becomes irregular so that at a given time the petals have attained different stages of development. Energy is absorbed essentially by plastic flow of the tubing material and by contact friction. The energy absorbed by the fracture process is small in comparison with that absorbed by plastic flow and friction.

The purpose of this paper is to develop a theoretical analysis to determine the force level in the tube and whether or not the petals will break off. A quasi-static process is assumed, i.e., inertia terms are neglected in the equations of motion. This means that the analysis is appropriate only when the maximum kinetic energy associated with the deformation of the tube is small in comparison with the total energy absorbed and the velocities are small in comparison with the elastic wave propagation speed.

McGehee [1][3] has conducted experiments on the fragmentation of 2024-T3 aluminum alloy tubing.

---

[3]Numbers in brackets refer to references listed at the end of the paper.

II Analysis of Petal Growth

Formulation of the Problem

The theoretical analysis of the growth of petals or cracks is based on seven assumptions. These assumptions follow.

a At a given instant all petals have the same configuration. This assumption is appropriate if one wishes to determine the force in the tube due to deformation of one petal or the average force in the tube. The theoretical peak tube stresses found from the following theoretical analysis occur only before the irregular process develops.

b The propagation of meridianal cracks is governed by a condition of critical radial displacement at the crack tips; hence, the average circumferential strain along a circle passing through the meridianal crack tips is an empirical constant.

c The loading and deformation of the unsplit portion of the tube is axisymmetric. This assumption follows from a provided a sufficiently large number, say six or more, petals form.

d The assumptions of the theory of thin shells apply to the unsplit portion of the tube. This is probably the least accurate assumption made, since the tube thickness to radius ratios employed in [1] are not sufficiently small. However, without this assumption an analysis would be virtually impossible.

e The tube is homogeneous and is made of a rigid-perfectly plastic material which obeys the Tresca or maximum shear stress yield condition and associated flow rule. This assumption is reasonable provided the plastic strains are large in comparison with the elastic strain at yielding and the material has negligible work hardening and anisotropy.

f Geometry changes are small enough so that equations of equilibrium and compatibility of the unsplit portion of the tube are those of a cylindrical shell.

g Coulomb friction occurs at all points of contact.

In addition, the analysis requires two a priori conditions. These follow.

h Contact between the tube material and the die occurs only at the tips of the formed

petals.

i The current meridianal curvature of the petals was produced when that point currently in the petal was part of the plastically deforming shell. The petals are assumed to be rigid, i.e., have unloaded from a plastic state.

Figure 2(a) shows the cross section of the tube CHI with a petal TC at its end. Contact with the die occurs at point T'. The region CHI behaves as a semi infinite plastic cylindrical shell subjected to axisymmetric transverse shear and bending moment at C. For a development of the plastic analysis of such a shell refer to the Appendix. Figure 2(b) shows the free body diagram of the petal and tube.

The dimensionless lengths appearing in the analysis are normalized with respect to the shell parameter $\sqrt{AT}$. The dimensionless stress resultants n_x, n_θ, q, and m are defined in the Appendix and in the Nomenclature. ξ is a dimensionless position coordinate measured from the petal tip. The lengths $\ell = \widehat{TC}/\sqrt{AT}$, $p = \widehat{CH}/\sqrt{AT}$, and

$$g = \ell + p, \tag{1}$$

shown in figure 2(a) all change with time. The dimensionless radial displacement u, the slope angle φ, and the dimensionless meridianal curvature $\varkappa$ are functions of the position coordinate ξ and time. The subscripts t, c, and h refer to locations T, C, and H, respectively.

Let $u = u(\xi,\tau)$, where τ increases monotonically with the time. Since the material properties are time independent, any variable which increases monotonically with time may replace τ. From assumption b

$$u(\ell,\tau) = u_c = a\varepsilon_c, \text{ a constant} \tag{2}$$

where ε_c is the average circumferential strain at $\xi = \ell$.

From differentiating (2)

$$\frac{\partial u}{\partial \tau}(\ell,\tau)d\tau + \frac{\partial u}{\partial \xi}(\ell,\tau)d\ell = 0$$

or

$$\varphi\ (\ell,\tau) = -\frac{\partial u}{\partial \xi}\ (\ell,\tau) = \frac{\partial u}{\partial \tau}\ (\ell,\tau)\ \frac{d\,\tau}{d\,\ell} \tag{3}$$

The slope angle at a given material point in the plastic region is the sum of the initial slope angle $\varphi_o(\xi)$ and the additional slope developed by plastic flow during the crack growth process.

Thus

$$\varphi\ (\xi,\tau) = \varphi_o(\xi) + \int_o^{\tau} \frac{\partial \varphi}{\partial \beta}(\xi,\beta)\ d\ \beta \tag{4}$$

As is developed in the Appendix, the dimensionless velocity v, angular velocity ω, and curvature rate $\dot{\kappa}$ depend on the dimensionless position coordinate η measured from the plastic hinge and an arbitrary multiplier. At a given instant $\frac{\partial \varphi}{\partial \tau}(\xi,\tau)$ is proportional to $\omega(\eta)$ where $\eta = g - \xi$. Also, $\frac{\partial u}{\partial \tau}(\xi,\tau)$ is in the same proportion to $v(\eta)$. Then it follows that

$$\frac{\frac{\partial \varphi}{\partial \tau}(\xi,\tau)}{\frac{\partial u}{\partial \tau}(\ell,\tau)} = \frac{\omega(\eta)}{v(p)} \tag{5}$$

Now let $\tau \equiv \ell$. The solutions show that ℓ increases monotonically with time; hence, this step is admissible. Substitute (5) and (3) into (4), and let $\xi = \ell$ to obtain

$$\varphi_c(\ell) = \varphi_o(\ell) + \int_o^{\ell} \frac{\omega[\,g(s) - \ell\,]}{v\,[p(s)]}\ \varphi_c(s)ds \tag{6}$$

From the relationship

$$\frac{\frac{\partial \varkappa}{\partial \tau}(\xi,\tau)}{\frac{\partial u}{\partial \tau}(\ell,\tau)} = \frac{\dot{\varkappa}(\eta)}{v(p)} \tag{7}$$

one finds an integral expression for $\varkappa_c$

$$\varkappa_c(\ell) = \varkappa_o(\ell) + \int_o^{\ell} \frac{\dot{\varkappa}[g(s) - \ell]}{v[p(s)]} \varphi_c(s)ds \tag{8}$$

Since the petals remain rigid, the curvature of the petals is

$$\varkappa(\xi) = \varkappa_c(\xi) \tag{9}$$

Into (6) and (8) are substituted expressions for the spacial distributions of the dimensionless radial velocity, angular velocity, and curvature rate in a rigid-plastic shell subjected to axisymmetric bending moment and shear force at its end. In the equations which follow the approximate expressions for v, ω, and $\dot{\varkappa}$ (equations (83), (84), and (85), respectively, of the Appendix) are used in place of the exact expressions derived in the Appendix. This produces some simplification at the expense of only slight errors. Since the variable p is always positive, one may omit the Heaviside function as a factor in $v[p(s)]$. One then obtains

$$\varphi_c(\ell) = \varphi_o(\ell) + (1 - \tfrac{2}{3}\sqrt{3}\ell) \int_o^{\ell} f(s)\cdot H[g(s)-\ell]ds + \tfrac{2}{3}\sqrt{3} \int_o^{\ell} f(s)\cdot g(s)\cdot H[g(s) -\ell]ds \tag{10}$$

$$\varkappa_c(\ell) = \varkappa_o(\ell) + \int_o^{\ell} f(s)\cdot\delta[g(s) - \ell]ds + \tfrac{2}{3}\sqrt{3} \int_o^{\ell} f(s)\cdot H[g(s) - \ell]ds \tag{11}$$

where

$$f(s) = \frac{\varphi_c(s)\cdot H(s)}{p(s) + \frac{1}{3}\sqrt{3}[p(s)]^2} \tag{12}$$

The definite integrals having the Heaviside step function and the Dirac delta function as factors of the integrands are evaluated by the following formulas:

$a < b$

$$\int_a^b f(x)\cdot H[g(x) - c]\,dx = \begin{cases} \int_a^b f(x)dx, & c < g(a) \\ \int_{g^{-1}(c)}^b f(x)dx, & g(a) \leq c \leq g(b) \\ 0\ , & c > g(b) \end{cases}$$

$$\int_a^b f(x)\cdot \delta[g(x) - c]\,dx = \begin{cases} 0\ , & c > g(a) \\ f[g^{-1}(c)]\left.\frac{dx(g)}{dg}\right|_{g=c}, & g(a) < c < g(b) \\ 0\ , & c > g(b) \end{cases}$$

where g^{-1} is the inverse of the function g, i.e. if $y = g(x)$, then $x = g^{-1}(y)$. Equations (10) and (11) become

$$\varphi_c(\ell) = \varphi_o(\ell) + (1 - \tfrac{2}{3}\sqrt{3}\,\ell)\int_{\ell^*}^{\ell} f(s)ds + \tfrac{2}{3}\sqrt{3}\int_{\ell^*}^{\ell} f(s)\cdot g(s)ds \tag{13}$$

$$x_c(\ell) = x_o(\ell) + f(\ell^*)\frac{d\ell^*}{d\ell} + \frac{2}{3}\sqrt{3}\int_{\ell^*}^{\ell} f(s)ds \tag{14}$$

where, with p_o the initial value of p, the lower limit ℓ^* satisfies

$$\begin{aligned} \ell^* &= 0 && \ell < p_o \\ \ell^* &= g^{-1}(\ell) && \ell \geq p_o \end{aligned} \tag{15}$$

The $\xi - \ell$ diagram of figure 3 aids the understanding of equations (13), (14), and (15). The line OT represents the ξ-coordinate of the petal tip, OA that of the crack tip, and $H^oH^*H^sHA$ the plastic hinge in the shell as ℓ increases from zero. The region to the left of OA is the petal. That between OA and $H^oH^*H^sHA$ is the plastic region in the shell, and that to the right of $H^oH^*H^sHA$ is rigid. Lengths shown in the diagram are

$$OT = TC = \ell\ ,\quad TH = g(\ell),\quad CH = g(\ell) - \ell = p(\ell)$$

$$OT^s = s,\quad T^sH^s = g(s),\quad BH^s = g(s) - \ell \geq 0$$

$$OT^* = \ell^*,\quad T^*H^* = g(\ell^*) = TC = \ell$$

$$OH^o = OT^o = p_o = g_o$$

A vertical line in the diagram represents states through which a material point must pass. If the crack tips have not reached the point C^o, then the material point currently at the crack tip was plastic at the time when the crack began to grow. In this case plastic deformation at the material point occurs during the time interval from 0 to ℓ. Thus, the lower limit of the integral is $\ell^* = 0$. After the crack tips have passed point C^o to point C, the material point currently at C was initially rigid. It underwent no plastic deformation until the plastic hinge reached that point. Thus,

the lower limit of the integrals must be the crack length at the instant the point currently at C became plastic. In the diagram this length is $\ell^* = OT^*$, found by dropping a vertical line from C to H^* and then drawing the horizontal line T^*H^*. Since the equation of the line $H^oH^*H^sH$ is $\xi = g(\ell)$ or $\ell = g^{-1}(\xi)$, then $\ell^* = g^{-1}(\ell)$. The shape of curve $H^oH^*H^sHA$ shown is typical for many computed cases.

As it is shown in the Appendix, the dimensionless length of the plastic region depends on the ratio of the applied bending moment to applied shearing focus. This ratio depends on the instanteous geometry and rate of change of geometry of the petal. The following shows how to find the instantaneous configuration.

From the condition that the petal is rigid one finds the slope angle $\varphi(\xi,\ell)$ at any point in the petal to be

$$\varphi(\xi,\ell) = \varphi_c(\ell) + \int_{\xi}^{\ell} \varkappa_c(\xi)\, d\,\xi \tag{16}$$

The tip slope angle $\varphi_t(\ell)$, tip radial displacement $u_t(\ell)$ and the projection $z_t(\ell)$ of the petal center line ($\overline{TC}$ of figure 2(a)) on the tube axis are

$$\varphi_t = \varphi_c + \int_o^{\ell} \varkappa_c(s)ds \tag{17}$$

$$u_t = u_c + \int_o^{\ell} \sin\,[\varphi\,(\xi,\ell)]\; d\,\xi \tag{18}$$

$$z_t = \int_o^{\ell} \cos[\varphi(\xi,\ell)]\; d\,\xi \tag{19}$$

Since a numerical technique will eventually be used to obtain solutions, it is more convenient to put equations (17), (18), and (19) in derivative forms rather than integral forms. Taking the derivative of φ_t with respect to ℓ and substituting (13) and (14) for φ_c and $\varkappa_c$ results in

$$\frac{d\varphi_t}{d\ell} = \left[1 + \frac{2}{3}\sqrt{3}\, p(\ell)\right] f(\ell) \tag{20}$$

By taking the derivative of u_t and z_t with respect to ℓ and noting that for a rigid petal

$$\frac{d}{d\ell}\varphi(\xi,\ell) = \frac{d\varphi_t}{d\ell}$$

one finds

$$\frac{du_t}{d\ell} = \sin\varphi_c + z_t \frac{d\varphi_t}{d\ell} \tag{21}$$

$$\frac{dz_t}{d\ell} = \cos\varphi_c - (u_t - u_c)\frac{d\varphi_t}{d\ell} \tag{22}$$

Let the projection of $\overset{\frown}{T'B}$ (figure 2(a)) on a radial line be $u_t'(\ell)$. Then, provided there is neither clearance nor interference between the tube and die entrance guide and the dimensionless die radius R is constant, the die angle ψ must satisfy

$$u_t' = R(1 - \cos\psi)$$

or

$$\psi = 2\arcsin\sqrt{\frac{u_t'}{2R}} \tag{23}$$

From geometry u_t' depends on u_t and φ_t.

$$u_t' = u_t + h(1-\cos\varphi_t) \tag{24}$$

The ratio of shearing force to bending moment at the crack tip depends on the geometry of the petal and die and the friction angle (figure 2(b)). This ratio becomes

$$2b = \frac{q_c}{m_c} = \frac{\cos(\nu - \varphi_c)}{(z_t + h \sin \varphi_t)\cos \nu + (u_t - u_c - h \cos \varphi_t) \sin \nu} \tag{25}$$

where

$$\nu = \psi + \tan^{-1} \mu \tag{26}$$

Finally, one obtains another expression relating b and p from equations (80) and (81) of the Appendix with $\eta = p$.

$$2b = \frac{q_c}{m_c} = \frac{2(p + \frac{1}{3}\sqrt{3}\, p^2)}{1 - p^2 - \frac{2}{9}\sqrt{3}\, p^3} \tag{27}$$

Fourteen variables (ℓ, p, q, φ_c, $\varkappa_c$, f, ℓ^*, φ_t, u_t, z_t, u_t', ψ, ν, and b) and thirteen functional relationships [equations (1), (12) through (15), and (20) through (27)] have been introduced. The constant parameters of the problem are R, h, u_c, and μ. The functions $\varphi_o(\xi)$ and $\varkappa_o(\xi)$ specify the initial state. The seven variables p, $\varkappa_c$, f, ν, u_t', ψ, and b may be eliminated by algebraic processes, leaving six coupled functional relationships among the remaining variables.

Solution

It is most convenient to treat ℓ as the independent variable. A numerical step-by-step method of solution, beginning at $\ell = 0$ and advancing by small steps $\Delta\ell$, has been developed. The method employs the trapezoid rule of integration and reiteration of each step until successive values of all variables agree within a specified percentage error. It is desirable to decrease the size of the step $\Delta\ell$ as the integration proceeds because as p becomes small f becomes large. In the

numerical procedure an initial value of $\Delta\ell$ is chosen, and $\Delta\ell$ is halved whenever the value of f increases by more than a specified percentage over one step. As p approaches zero, the behavior becomes singular; therefore, the procedure must be terminated when p becomes small. Then an asymptotic solution employing a variable other than ℓ as the independent variable is used. This asymptotic method is described later.

The method was programed in the Fortran language for an IBM 7070 computer. After a few trials, it was found that satisfactory results were obtained by choosing $\Delta\ell = 0.1$ initially, halving $\Delta\ell$ when f changed by more than 25%, and reiterating to an accuracy of 0.3%. The procedure was terminated when either p became less than .03 or $\Delta\ell$ became less than .0005. The functions chosen for φ_o and $\varkappa_o$ are the dimensionless slope and curvature resulting from the application of a transverse shear force at the end of the tube to open it up by a radial amount u_c.

Asymptotic Method for Small p

From the differentiation of (13) and (14) with respect to ℓ and the condition that p is small one finds

$$\frac{d\varphi_c}{d\ell} \approx \frac{d\varphi_o}{d\ell} + \frac{\varphi_c}{p}$$

$$\frac{d\varkappa_c}{d\ell} \approx \frac{d\varkappa_o}{d\ell} + \frac{2}{3}\sqrt{3}\frac{\varphi_c}{p}$$

In general, where the asymptotic solution applies, $\varphi_o(\ell)$ and $\varkappa_o(\ell)$ vanish. Let this be the case. Now with φ_c as the independent variable,

$$\frac{d\varkappa_c}{d\varphi_c} \approx \frac{2}{3}\sqrt{3} \qquad (28)$$

$$\frac{d\,\ell}{d\varphi_c} \approx \frac{p}{\varphi_c} \tag{29}$$

By changing the independent variable from ℓ to φ_c in (20), (21), and (22) and employing (29) one finds

$$\frac{d\varphi_t}{d\varphi_c} \approx 1 \tag{30}$$

$$\frac{du_t}{d\varphi_c} \approx z_t \tag{31}$$

$$\frac{dz_t}{d\varphi_c} \approx u_t - u_c \tag{32}$$

For small p equation (27) reduces to

$$b \approx p \tag{33}$$

One must now solve the eight coupled functional relationships (23) through (26) and (30) through (33) for eight dependent variables φ_t, u_t, z_t, p, b, u_t', ψ, and ν as functions of the independent variable φ_c. Again a numerical step-by-step procedure employing the trapezoid integration rule and reiteration is used. The initial data for this computation is, of course, taken from the final step of the previous computation. A step of $\Delta\varphi_c = 0.05$ was used. The procedure is repeated until p becomes zero. Both ℓ and $\varkappa_c$ may be calculated afterward from (28) and (29). Equation (29) shows that the cracks are arrested when p reaches zero, i.e., the crack tips and plastic hinges have the same ξ-coordinate and the shearing force at the petal bases vanishes.

III Petal Bending with Stationary Cracks

After the crack has been arrested, the plastic hinge moves away from the crack tip into the petal. Figure 4(a) shows a cross section of the petal with the plastic hinge at point H, the crack tip being at point C. It is assumed that the petal behaves as a plastic curved beam subjected to tip loading. The bending moment is a maximum at $\xi = g$, the location of the plastic hinge. The shear force vanishes at $\xi = g$; hence, from figure 4(b)

$$\psi + \tan^{-1}\mu - \varphi_h = \tfrac{1}{2}\pi \ . \tag{34}$$

For a constant friction coefficient

$$\frac{d\psi}{d\varphi_h} = 1 \ . \tag{35}$$

A change in the slope angle $\Delta\varphi_h$ at the plastic hinge is the sum of a rigid body rotation $\Delta\varphi_t$ of the region between the hinge and the petal tip and a change $-\varkappa\Delta g$ due to the movement Δg of plastic hinge along the petal with curvature $\varkappa$. In derivative form this condition becomes

$$\frac{d\varphi_t}{d\varphi_h} - \varkappa \frac{dg}{d\varphi_h} = 1 \ . \tag{36}$$

Other geometrical relationships are

$$\frac{du_t}{d\varphi_h} = y \frac{d\varphi_t}{d\varphi_h} \tag{37}$$

$$\frac{dy}{d\varphi_h} = \frac{dg}{d\varphi_h} \cos \varphi_h - (u_t - u_h) \frac{d\varphi_t}{d\varphi_h} \tag{38}$$

$$\frac{du_h}{d\varphi_h} = -\frac{dg}{d\varphi_h} \sin \varphi_h \tag{39}$$

where y is the axial projection of line TH of figure 4(a) and u_h is the total radial displacement at the plastic hinge. The die contact angle ψ is related to the radial displacement at the petal tip by equations (23) and (24). Now substituting (24) into (23), differentiating with respect to φ_h, using the result of (35), and rearranging, one finds

$$\frac{d\varphi_t}{d\varphi_h} = \frac{R \sin \psi}{y + h \sin \varphi_t} \quad . \tag{40}$$

Then from (36) and (40)

$$-\frac{dg}{d\varphi_h} = \frac{1}{\kappa} \left[1 - \frac{R \sin \psi}{y + h \sin \varphi_t} \right] . \tag{41}$$

In (41) κ is the curvature of the petal just ahead of the moving hinge. Its value is obtained from the solution of the crack growth problem.

The system of six differential equations (35) and (37) through (41) can be solved for the six variables ψ, φ_t, g, u_t, y, and u_h as functions of φ_h. The trapezoid rule of numerical integration and reiteration of each step to a desired accuracy have been used to obtain step-by-step numerical solutions. The initial data used for these calculations is the terminal data taken from the solution of the crack growth problem.

IV Load-Displacement Behavior

Since it has been assumed that contact between the tube material and the die occurs only at the petal tips, the axial force per unit circumference in the rigid tube depends only on the magnitude of the die contact force F per unit circumference of undeformed tube and the angle ν. The compressive stress in the tube is

$$\frac{\sigma}{\sigma_o} = \frac{F}{\sigma_o T} \sin \nu \ . \tag{42}$$

For the crack propogation problem one finds F by eliminating m_c from the expressions

$$4m_c = 1 - p^2 - \frac{2}{9} \sqrt{3}\, p^3 \tag{43}$$

and

$$m_c = \frac{F\sqrt{AT}}{\sigma_o T^2} [(z_t + h \sin \varphi_t) \cos \nu + (u_t - u_c - h \cos \varphi_t) \sin \nu] \tag{44}$$

or by eliminating q_c from the expressions

$$2q_c = p + \frac{1}{3} \sqrt{3}\, p^2 \tag{45}$$

and

$$q_c = \frac{F\sqrt{AT}}{\sigma_o T^2} \cos (\nu - \varphi_c). \tag{46}$$

After the crack has been arrested, the condition that $4m_h = 1$ yields the result

$$\frac{F\sqrt{AT}}{\sigma_o T^2} = \frac{0.25}{(y + h \sin \varphi_t) \cos \nu + (u_t - u_n - h \cos \varphi_t) \sin \nu} \ . \tag{47}$$

The meridianal membrane stress at the petal root is

$$n_{xc} = -\frac{F}{\sigma_o T} \sin(\nu - \varphi_c) \ . \tag{48}$$

The yield condition used so far is independent of this stress. Such a condition is valid provided $|n_{xc}|$ is small in comparison with one. For the present problem this is not always the case; therefore, a correction for this effect is needed. To obtain an approximate correction, assume that the effect of n_x on the projection of the yield surface on the m, n_θ plane is to change only the size but not the shape of the figure. The plastic analysis of such a cylindrical shell is given in the Appendix. The intersection of the m-axis and the yield surface is given by

$$4m = 1 - n_x^2$$

hence, the size factor for the yield surface is assumed to be $1 - n_x^2$. For such a yield surface m and q of equations (69) and (70) are replaced by $m/(1 - n_x^2)$ and $q/(1 - n_x^2)$, respectively. To employ such a yield surface in the crack propagation analysis, replace m_c in equation (43) by $m_c/(1 - n_{xc}^2)$ and q_c in equation (45) by $q_c/(1 - n_{xc}^2)$. The above approximate yield surface is expected to give results very close to those obtained from the exact Tresca yield surface because the effect of $|n_{xc}|$ on the yield surface becomes appreciable only when the generalized stress profile approaches the m-axis, where the exact and approximate yield surfaces coincide. To apply the approximate correction for axial force to the stationary crack problem, multiply the numerator on the right hand side of equation (47) by $(1 - n_{xh}^2)$ where

$$n_{xh} = -\frac{F}{\sigma_o T} \ . \tag{49}$$

The compressive stress in the tube found by employing the axial force dependent yield surface is denoted by σ'.

Let D denote the dimensionless displacement of the undeformed part of the tube relative to the die and take $D = 0$ when the tip enters the curved part of the die. It is assumed that there is neither clearance nor interference between the tube and the die, entrance and that meridianal lines on the tube middle surface do not change in length. From geometry of the crack growth problem

$$D = \ell - z_t - h \sin \varphi_t + R \sin \psi \ . \tag{50}$$

For the problem of petal bending with stationary cracks the derivative of D with respect to the independent variable is

$$\frac{dD}{d\varphi_h} = R \cos \psi + (u_t - u_h - h \cos \varphi_t) \frac{d\varphi_t}{d\varphi_h} \ . \tag{51}$$

The rigid tube displacement relative to the die is then found by numerical integration.

V A Theoretical Analysis of the Rolling Process

For small t/R ratios the a priori condition h does not hold. In this case the petals formed are likely to roll up to a radius close to the die radius. This phenomenon is called rolling. In the following analysis it is assumed that, when rolling occurs, the flow of material in the deforming region is steady and that the curvature of the formed petal corresponds to the die radius. The satisfaction of both of these conditions places some restrictions upon the die configuration near the entrance. This restriction will be discussed later. Figure 5 shows the petals bent to the die radius. The plastic analysis of cylindrical shells of the Appendix applies to the deforming portion of the tube. The tube material flows steadily along a path, entering the deforming region at $\eta = 0$ and leaving at $\eta = \eta_c$, the coordinate at the crack tip or petal base. Here η is the dimensionless coordinate of a point of the deforming tube measured in a frame of reference fixed to the die. The point at which plastic deformation commences is the origin. When axial compression is neglected, the average axial velocity over the cross section is independent of η. The time τ required for a material point entering the deforming region at $\eta = 0$ to reach the position η is proportional to η. Then

$$\tau = \frac{\eta}{w} \tag{52}$$

where w is the dimensionless velocity of the tube relative to the die. The dimensionless radial displacement u of a point at η is found by integrating the radial velocity v with respect to time. The dependence of the radial velocity on the coordinate η is given by equation (77) or (83) in the Appendix. For steady flow Λ must be independent of η. The expression for the radial displacement becomes

$$u\,[\eta\,(\tau)] = \int_0^{\tau} v\;\;[\eta(\tau)]\;d\tau$$

or

$$u\,(\eta) = \frac{1}{w}\int_0^{\eta} v\,(\eta)\,d\eta\,. \tag{53}$$

From equations (77) of the Appendix and (53)

$$u\,(\eta) = \lambda'\,(\tfrac{1}{2}\,\eta^2 + \frac{1}{6}\,\eta^3 + \frac{1}{72}\,\eta^4)\;H\,(\eta) \tag{54}$$

where $\lambda' = \Delta/w$. Expressions for the slope and the curvature are found by differentiation with respect to η . Thus

$$\varphi\,(\eta) = \lambda'\,(\eta + \tfrac{1}{2}\,\eta^2 + \frac{1}{18}\,\eta^3)\;H\,(\eta) \tag{55}$$

$$\varkappa\,(\eta) = \lambda'\,(1 + \eta + \frac{1}{6}\,\eta^2)\;H\,(\eta)\,. \tag{56}$$

Two conditions are maintained at $\eta = \eta_c$. They are that the petal curvature corresponds to the die radius and that the radial displacement is that which is required to maintain the crack. These two conditions are expressed by

$$\varkappa_c = \lambda'\,(1 + \eta_c + \frac{1}{6}\,\eta_c{}^2) = \frac{1}{R - h} \tag{57}$$

$$u_c = \lambda'\,(\tfrac{1}{2}\,\eta_c{}^2 + \frac{1}{6}\,\eta_c{}^3 + \frac{1}{72}\,\eta_c{}^4) = a\varepsilon_c\,. \tag{58}$$

η_c and λ' are found by solving equations (57) and (58) simultaneously.

The slope of both the die and the petal must be the same at point C if the petal is to match the die exactly. This cannot be the case if the die radius is constant. If the die radius is modified along the arc $\overset{\frown}{BC'}$ as shown in Figure 6,

the condition of matching slopes is satisfied. For slopes satisfying $\varphi_c \ll 1$

$$u_c = \tfrac{1}{2} (R_1 - h) \varphi_c^2$$

from which

$$\frac{R_1 - h}{R - h} = \frac{2 u_c \kappa_c}{\varphi_c^2} \quad . \tag{59}$$

The numerical value of $(R_1 - h)/(R - h)$ lies between 1.0 and 1.2; therefore, dies by which steady state formation of petals of constant curvature may be achieved are almost constant radius dies.

Figure 7 shows a free body diagram of the petal which may carry an arbitrary distribution of contact force $\bar{p}$ and a friction force $\mu\bar{p}$. If there is no friction, the tangential force must vanish. For the frictionless die

$$N_c = - \int_{\varphi_c}^{\varphi_t} R\bar{p} \sin (\varphi - \varphi_c) \, d\varphi = - \frac{M_c}{R - h} \quad .$$

In terms of dimensionless variables

$$n_c = - m_c \frac{t}{R - h} \tag{60}$$

where m_c is found from equation (69) of the Appendix, with $\eta = \eta_c$. The stress in the undeformed tube is

$$\frac{\sigma}{\sigma_o} = - n_c \cos \varphi_c + \frac{q_c}{t} \sin \varphi_c \tag{61}$$

where q_c is found from equation (70) of the Appendix. With some algebraic

manipulation equation (61) reduces to

$$\frac{\sigma}{\sigma_o} = \tfrac{1}{4} \frac{t}{R - h} + \tfrac{1}{2} \left(1 + \frac{1}{3} \eta_c + \frac{1}{18} \eta_c^2\right) \varepsilon_c \ . \tag{62}$$

For practical values of η_c the factor in parentheses in (62) has a value in the range 1.0 to 1.33. A limitation of the foregoing analysis is that ε_c must satisfy $\varepsilon_c < \frac{1}{4}\, t/(R - h)$.

For $\varepsilon_c > \frac{1}{4}\, t/(R - h)$ a portion of the unsplit but deformed tube has contact with the die. Again shell theory is used to determine the stress in the tube. The resulting expression for the stress in the tube is

$$\frac{\sigma}{\sigma_o} = \varepsilon_c + \frac{1}{6} \frac{t}{R - h} \ . \tag{63}$$

The details of this calculation are omitted here for brevity.

When a small coefficient of friction (about .2 or less) between the die and petal exists, equation (60) must be replaced by

$$n_c = - m_c \frac{t}{R - h} - \mu \frac{R}{R - h} \sqrt{\left(m_c \frac{t}{R - h}\right)^2 + \frac{t}{a} q_c^2} \ . \tag{64}$$

Equation (64) is not an exact expression, but contains only the first order terms in μ. The derivation of equation (64) is omitted for brevity. Figure 8 shows the results of calculations.

VI Theoretical Results and Comparison with Experiment

Geometric results of a sample calculation are shown in Figure 9. The data $a/R = 1.75$, $t/R = .6$, and $\varepsilon_c = .02$ are typical values for the tube fragmentation tests of reference [2] using 2024 - T3 aluminum alloy as the tubing material. The value for ε_c was obtained from measurements of deformed specimens of these tests. The friction coefficient is assumed to vanish corresponding to a well lubricated die. Figure 10 shows how the ξ-coordinate of the plastic hinge g and that of the crack tip ℓ change as the tube is pushed over the die. Figure 10 also shows the load-displacement behavior of the rigid tube. In Figures 9 and 10 the dotted lines at the left show interpolations to the known initial data for $D = 0$. The interpolation line for φ_h vs. D in Figure 9 begins at the value of D for which g reaches a maximum as would be expected. The area under the σ/σ_o vs. D curve in Figure 10 represents the energy absorbed during the fragmentation process. The maximum ordinate of the σ'/σ_o vs. D curve indicates the maximum compressive stress reached in the undeformed part of the tube. Buckling of the tube as a short column may occur if σ'/σ_o becomes too large. For the buckling problem it is necessary to treat the tube material as an elastic-work hardening material. The buckling problem is not considered in this paper.

Figures 11(a) and 11(b) show the petal shapes at the time when the crack becomes arrested and when the motion of the plastic hinge in the petal changes its direction. These figures show the highly non-uniform distribution of bending in the petals for this case. Transverse fracture of the petal is very likely when the configuration of Figure 11(b) is reached due to the large bending strains developed.

Figure 12 shows the effect of the ratio t/R on the load-displacement behavior of tubes pushed over a die. For the three cases shown, the constant data is $a/R = 1.75$, $\varepsilon_c = .02$, and $\mu = 0$. For the cases $t/R = .3$ and $t/R = .46$, condition h (that contact between the tube material and the die occurs only at

the tips of the formed petals) is valid only during the early stages of petal growth. The load-displacement behavior for these cases is shown only up to the displacement for which condition h holds. At larger displacements contact occurs at both the petal tip and over a circle in the unsplit portion of the tube. Continued displacement of the tube would, due to the new contact force, cause an increase of the shearing force on the unsplit portion of the shell. This in turn causes an increase of length of the plastic region in the unsplit portion of the tube. It is conjectured that then the length of the plastic region in the unsplit portion of the tube would reach a relative maximum and then decrease due to rapid running of the meridianal cracks. A theoretical analysis of this deformation would be too complicated to carry out; however, reasonable estimates of the force level in the undeformed tube may be obtained by supposing that the length of plastic region remains constant, i.e., by using the results for steady state rolling.

Figure 13 shows how a change in the ratio a/R affects the load-displacement behavior for $t/R = .46$, $\varepsilon_c = .02$, and $\mu = 0$. Figures 14 and 15 show how changing the friction coefficient from 0 to 0.2 affects the load-displacement behavior when $\varepsilon_c = .02$, $a/R = 1.75$, and $t/R = .46$ or $t/R = .6$. Note the large effect of friction when $t/R = .6$.

Results of tests of tubes of 2024 -T3 aluminum alloy have been communicated to the author [2]. Figure 16 shows the stress-strain behavior in compression for this material and that for a rigid perfectly plastic idealization with a flow stress of 60 ksi. The dotted lines of Figure 17 show the measured stress levels plotted as a function of $t/(R - h)$ for various values of $a/(R - h)$. These curves were plotted from an empirical expression given in [2] by taking the flow stress σ_o as 60,000 psi. The slight increase of σ'/σ_o with increasing $a/(R - h)$ is in agreement with the theoretical results of Figure 13. Curve 1 of Figure 17 shows

theoretical stress levels for steady state rolling and curve 2 shows that for fragmentation. For $.35 < t/(R - h) < .7$ agreement between the theoretical fragmentation stress and the measured stress is good. For larger $t/(R - h)$ the theory predicts a stress in the undeformed part of the tube which is much less than the measured values.

Some reasons for the difference are given in the following:

1. For large $t/(R - h)$ the theoretical analysis shows that the contact force at the petal tips becomes large, so that the edges would be crushed. The energy absorbed by local plastic flow and the change in petal shape due to this crushing have not been considered in the theoretical analysis.

2. The cross section of the petals is not rectangular in shape but is a sector of an annulus which has a greater plastic limit moment than the assumed rectangular section.

3. The dies were machined to have a slight interference with the inside of the tubular specimens along the die entrance guide. Considerable friction may occur along this contact surface.

4. The assumption that the length of the middle surface does not change is poorest for the case of large t/R; hence, the calculated values of D are too small.

VII Conclusions

1. In the fragmentation regime meridianally running cracks advance rapidly when the shearing force at the petal roots is large and become arrested when this shearing force vanishes.
2. Large localized bending strains develop; therefore, points where transverse fracture is likely to occur may be determined.
3. The direct stress in the tube increases with increasing t/R in both the fragmentation and the rolling regimes.
4. The direct stress in the tube increases slightly with increasing a/R.
5. The effect of friction on the force level in the undeformed part of the tube is significant.
6. The compressive stress in the undeformed part of the tube may reach peak values sufficiently large to cause column buckling of the tube unless the tube is supported laterally to prevent such buckling.
7. For large t/R the energy absorbed by crushing at the petal tips may be significant.

APPENDIX Plastic Analysis of a Cylindrical Shell

A semi-infinite cylindrical shell is subjected to the axisymmetric edge bending moment M and shearing force Q as shown in Figure 18(a). The coordinate x is measured from the point where the shearing force vanishes. The following dimensionless notation is introduced:

$$m = M/\sigma_o T^2 , \qquad q = Q\sqrt{AT}/\sigma_o T^2$$

$$n_\theta = N_\theta/\sigma_o T , \qquad n_x = N_x/\sigma_o T$$

$$\eta = x/\sqrt{AT} .$$

In terms of the dimensionless quantities, the equations of equilibrium are

$$\frac{dm}{d\eta} = -q \tag{65}$$

$$\frac{dq}{d\eta} = n_\theta \tag{66}$$

$$\frac{dn_x}{d\eta} = 0 . \tag{67}$$

When $n_x = 0$, $m \geq 0$, $n_\theta \geq \frac{1}{2}$, the Tresca yield condition [Figure 18(f)] for a cylindrical shell is (see reference [3])

$$\Phi\ (m, n_\theta) = 0$$

where

$$\Phi = 4m + (2n_\theta - 1)^2 - 1. \tag{68}$$

The solution to (65), (66), and (67) is

$$4m = 1 - \eta^2 - \frac{1}{3}\eta^3 - \frac{1}{36}\eta^4 \tag{69}$$

$$2q = \eta + \tfrac{1}{2}\eta^2 + \frac{1}{18}\eta^3 \tag{70}$$

$$n_\theta = \tfrac{1}{2} + \tfrac{1}{2}\eta + \frac{1}{6}\eta^2 \quad . \tag{71}$$

Figures 18(b), 18(c), and 18(d) show the variations of m, q, and n_θ with η. By eliminating η from equation (69) and (70) one obtains the first quadrant of the yield curve in load space shown in Figure 18(e).

For a cylindrical shell the generalized strain rates are the curvature rate $\dot{K}$ and the circumferential strain rate $\dot{\varepsilon}$. These generalized strain rates are related to the radial velocity V by

$$\dot{K} = \frac{d^2V}{dx^2} = \frac{1}{AT}\frac{d^2V}{d\eta^2} \tag{72}$$

$$\dot{\varepsilon} = \frac{V}{A} \quad . \tag{73}$$

The flow rule of the theory of plasticity states that the generalized strain rate vector points in the direction of the outward normal to the yield surface at a regular point. This means that

$$\dot{K} = \frac{\lambda}{\sigma_o T^2}\frac{\partial \Phi}{\partial m} \tag{74}$$

$$\dot{\varepsilon} = \frac{\lambda}{\sigma_o T}\frac{\partial \Phi}{\partial n_\theta} \tag{75}$$

where $\lambda \geq 0$.

Expression (68) is substituted into (74) and (75) and λ is eliminated to obtain a differential equation for V.

$$\frac{d^2V}{d\eta^2} = \frac{1}{2\,n_\theta - 1}\,V \quad . \tag{76}$$

Let $v = V/\sqrt{AT}$ be the dimensionless radial velocity, ω be the dimensionless angular velocity and $\dot{\varkappa} = \sqrt{AT}\,\dot{K}$ be the dimensionless curvature rate. The solution to (76) is

$$v = A(\eta + \tfrac{1}{2}\eta^2 + \frac{1}{18}\,\eta^3)\,H(\eta) \tag{77}$$

$$\omega = \frac{dv}{d\eta} = A(1 + \eta + \frac{1}{6}\eta^2)\,H(\eta) \tag{78}$$

$$\dot{\varkappa} = \frac{d\,\omega}{d\,\eta} = A\,[\delta(\eta) + (1 + \frac{1}{3}\eta)\,H(\eta)] \tag{79}$$

where $A \geq 0$, $H(\eta)$ is the Heaviside step function and $\delta(\eta)$ is the Dirac delta function.

Equation (71) shows that the variation of n_θ with η is almost linear. To obtain suitable approximations by polynomials of a lower order, assume that the variation of n_θ with η is linear, equations (65) and (66) hold, and that $n_\theta = \frac{1}{2}$ where $m = \frac{1}{4}$ and $n_\theta = 1$ where $m = 0$. The resulting approximations are

$$4m = 1 - \eta^2 - \frac{2}{9}\sqrt{3}\,\eta^3 \tag{80}$$

$$2q = \eta + \frac{1}{3}\sqrt{3}\,\eta^2 \tag{81}$$

$$n_\theta = 1 + \frac{2}{3}\sqrt{3}\,\eta \quad . \tag{82}$$

An approximate expression for the velocity field is found by observing the similarity of the exact expressions for v and 2q and applying this similarity to the approximate expression. Thus the approximate velocity field is

$$v = \Delta \left(\eta + \frac{1}{3}\sqrt{3}\eta^2\right) H(\eta) \tag{83}$$

$$\omega = \Delta \left(1 + \frac{2}{3}\sqrt{3}\,\eta\right) H(\eta) \tag{84}$$

$$\dot{\varkappa} = \Delta \left[\delta(\eta) + \frac{2}{3}\sqrt{3}\, H(\eta)\right] \tag{85}$$

When n_x is not zero the yield surface of a cylindrical shell of Tresca material subjected to axisymmetric loading has the form

$$\Phi_1 (m, n_\theta, n_x) = 0$$

An approximate expression for Φ_1, suitable for the region $n_\theta > 0$, $m > 0$, $n_x < 0$ but small, is

$$\Phi_1 = \frac{4m}{1 - n_x^2} + \left(\frac{2n_\theta}{1 - n_x^2} - 1\right)^2 - 1 \tag{86}$$

Φ_1 is obtained by replacing m and n_θ in the expression Φ by $\frac{m}{1 - n_x^2}$ and $\frac{n_\theta}{1 - n_x^2}$, respectively. The projection of $\Phi_1 = 0$ on the plane $n_x = -0.5$ is shown in figure 18(f). The plastic analysis involves the satifaction of equations (65), (66), (67), and (86). The solution is given by expressions (69), (70), and (71) with m, q, and n_θ replaced by $\frac{m}{1 - n_x^2}$, $\frac{q}{1 - n_x^2}$, and $\frac{n_\theta}{1 - n_x^2}$, respectively. Fig. 18 (e) shows such a yield curve in load space for $n_x = -.5$. For the approximate yield surface, the normality condition yields the transverse velocity field given by equations (77), (78), and

(79) with no changes.

The derivations and results of this Appendix were guided by [4].

Acknowledgement

The author wishes to thank Mr. J. R. McGehee of Langley Research Center, NASA, for discussions of the tube fragmentation process. The author also wishes to thank Professors D. C. Drucker and P. S. Symonds for discussions during the early part of the investigation.

References

1. McGehee, J. R. : A Preliminary Experimental Investigation of an Energy- Absorption Process Employing Frangible Metal Tubing. NASA TN D-1477, 1962.

2. NASA unpublished data.

3. Prager, W.: An Introduction to Plasticity. Addison Wesley Publishing Co., 1959.

4. Eason, G.: The Load Carrying Capacities of Cylindrical Shells Subjected to a Ring of Force. J. Mech. Phys. Solids, Vol. 7, pp. 169-181, 1959.

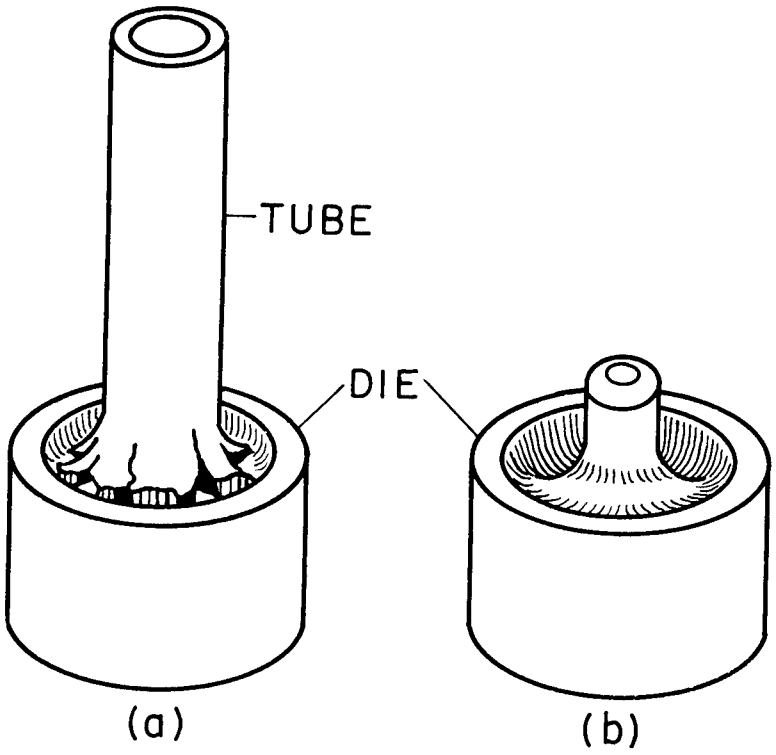

Fig. 1 (a) Fragmenting tube; (b) Die

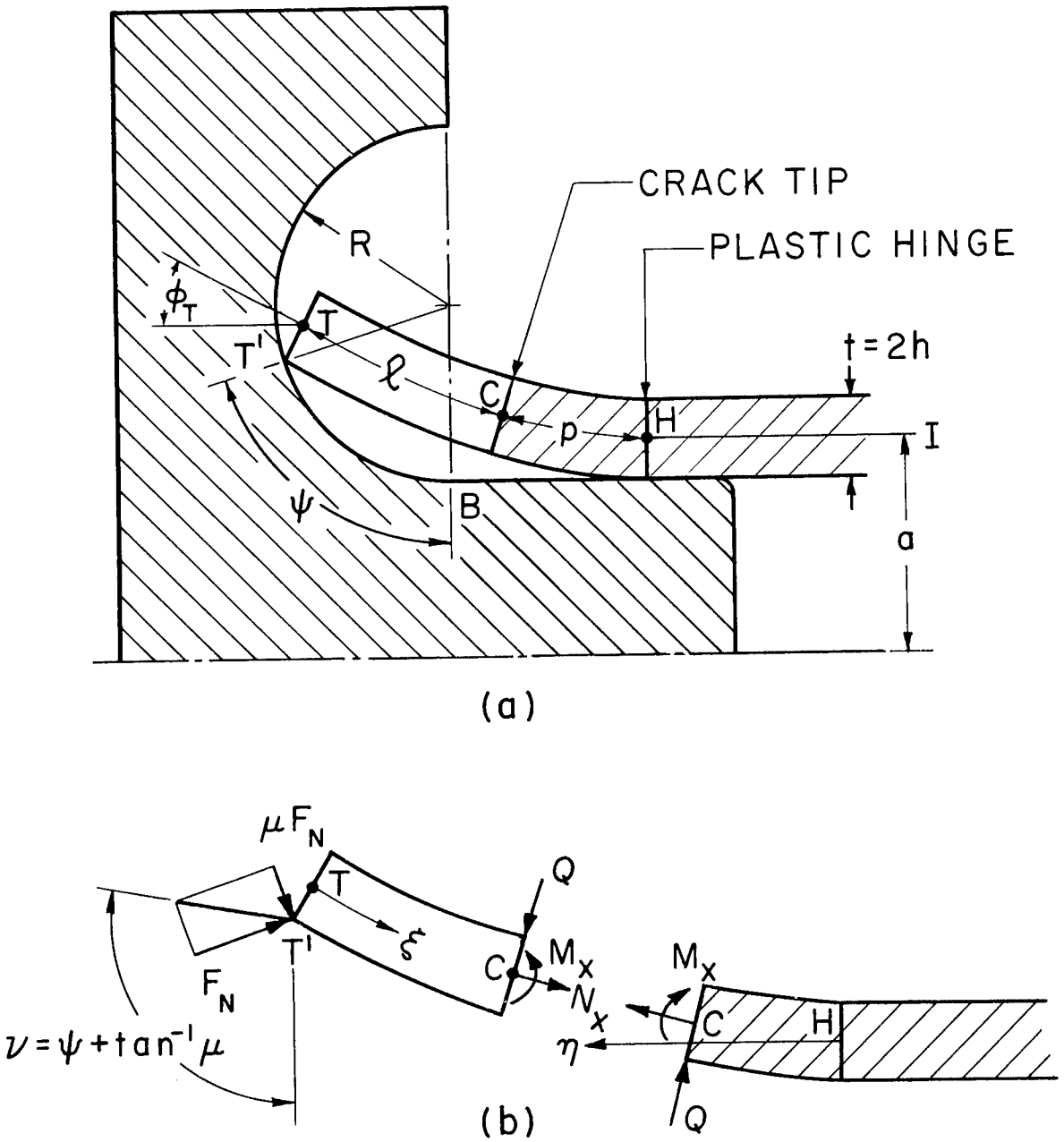

Fig. 2 (a) Cross section of tube, petal, and die during crack propagation;
(b) Free body diagram

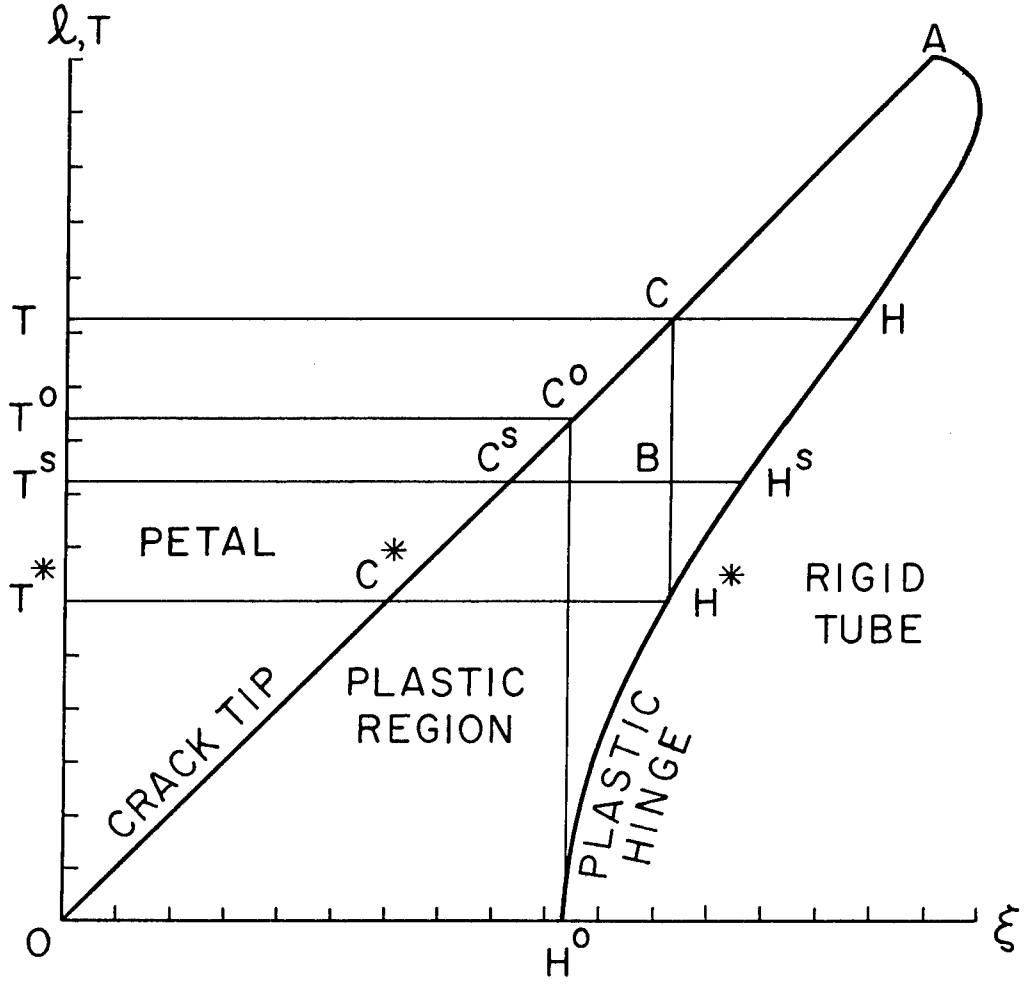

Fig. 3 $\xi - \ell$ diagram

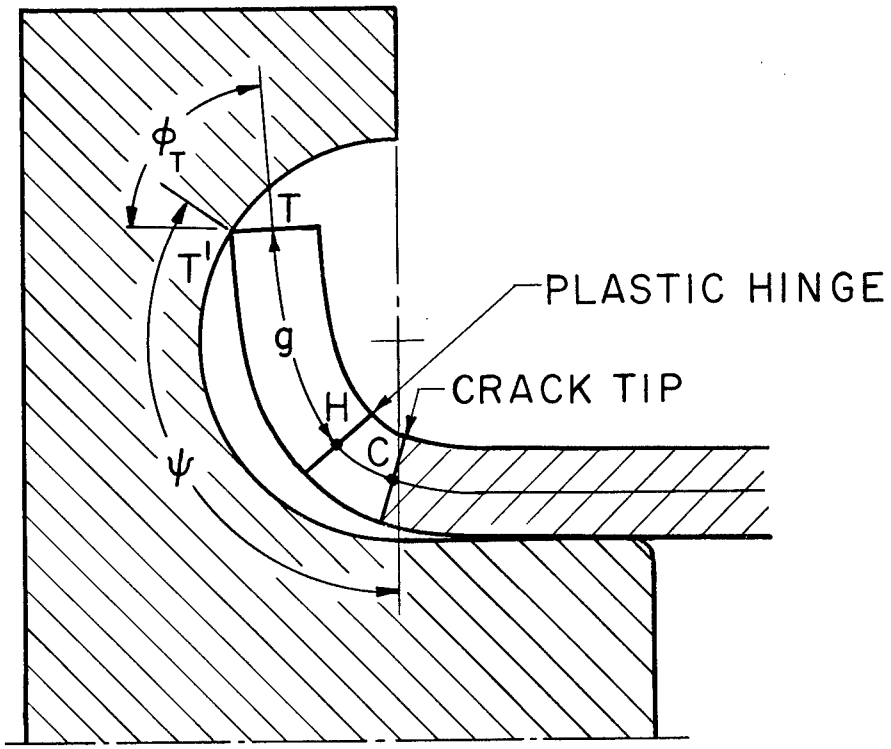

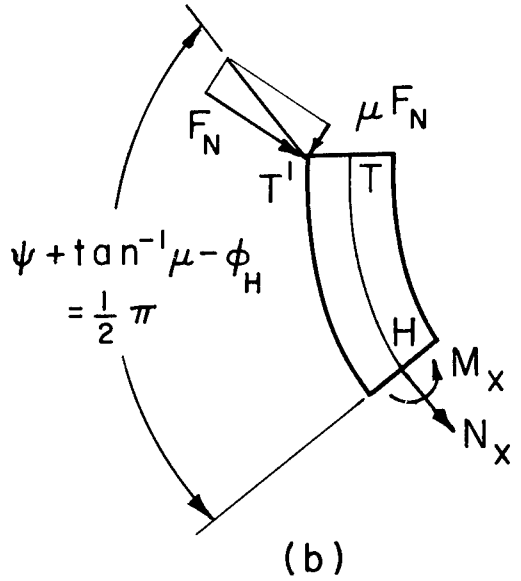

Fig. 4 (a) Cross section of tube, petal, and die during petal bending; (b) Free body diagram

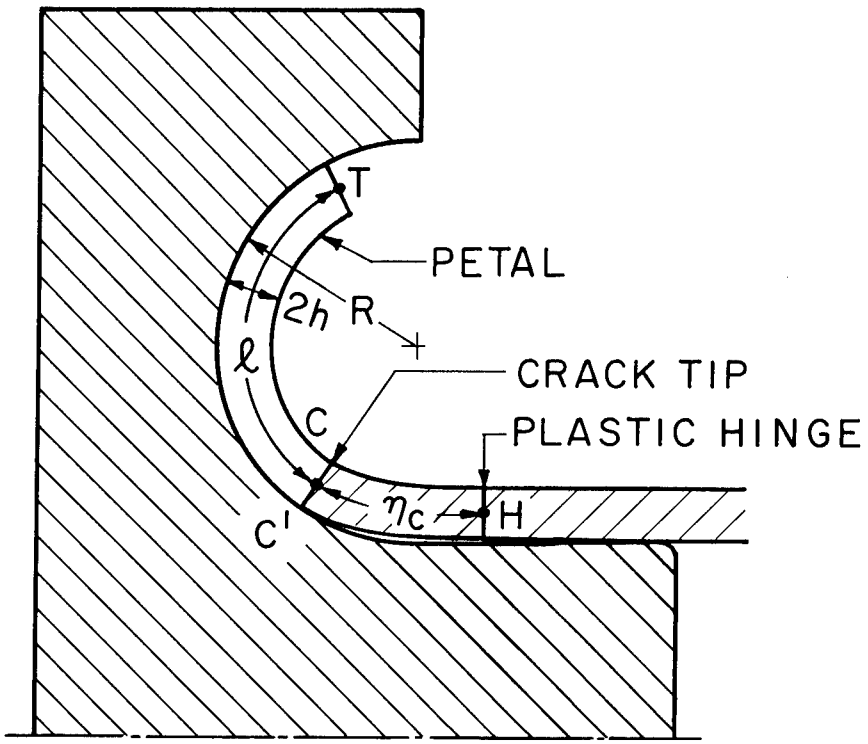

Fig. 5 Cross section of tube, petal, and die during rolling

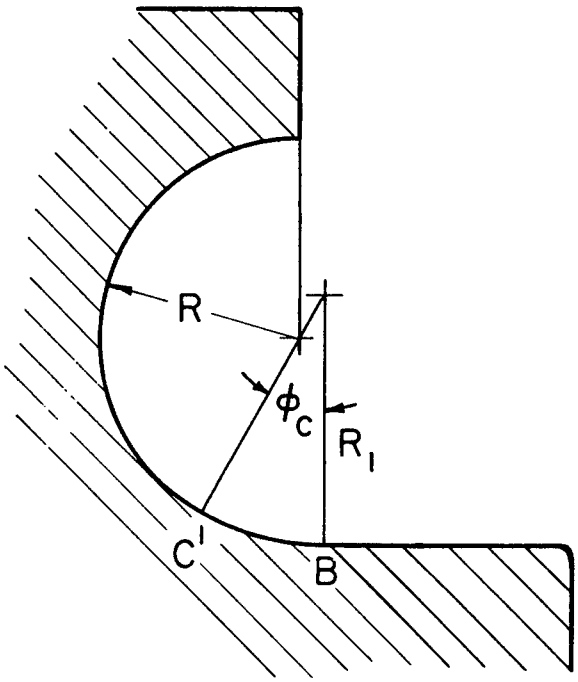

Fig. 6 Modified die profile

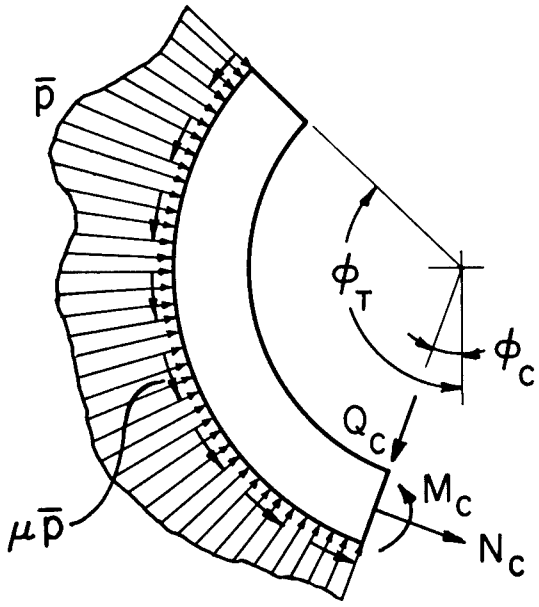

Fig. 7 Pressure and frictional loading on the petal during rolling

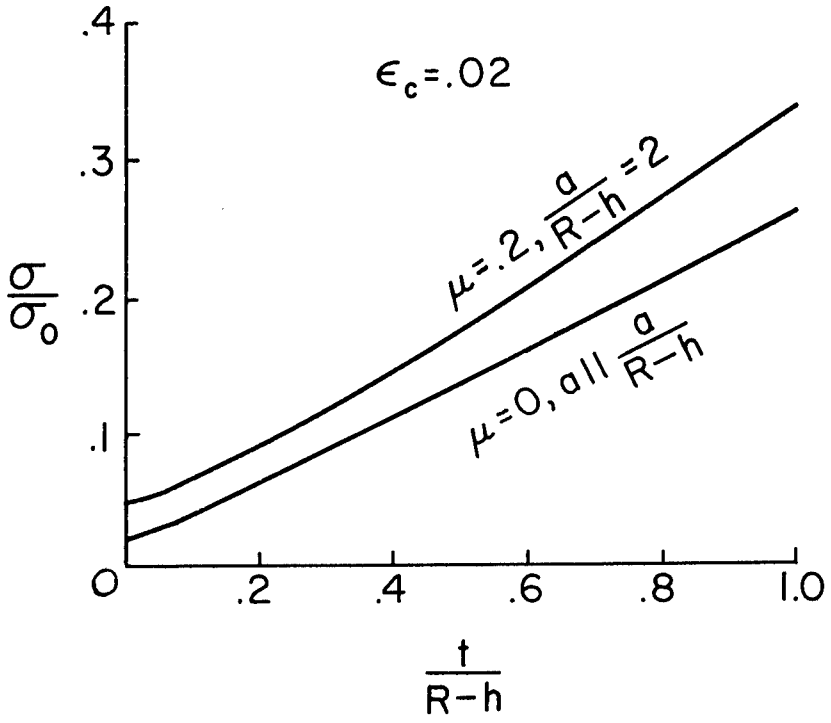

Fig. 8 Tube stress during rolling as a function of t/(R-h)

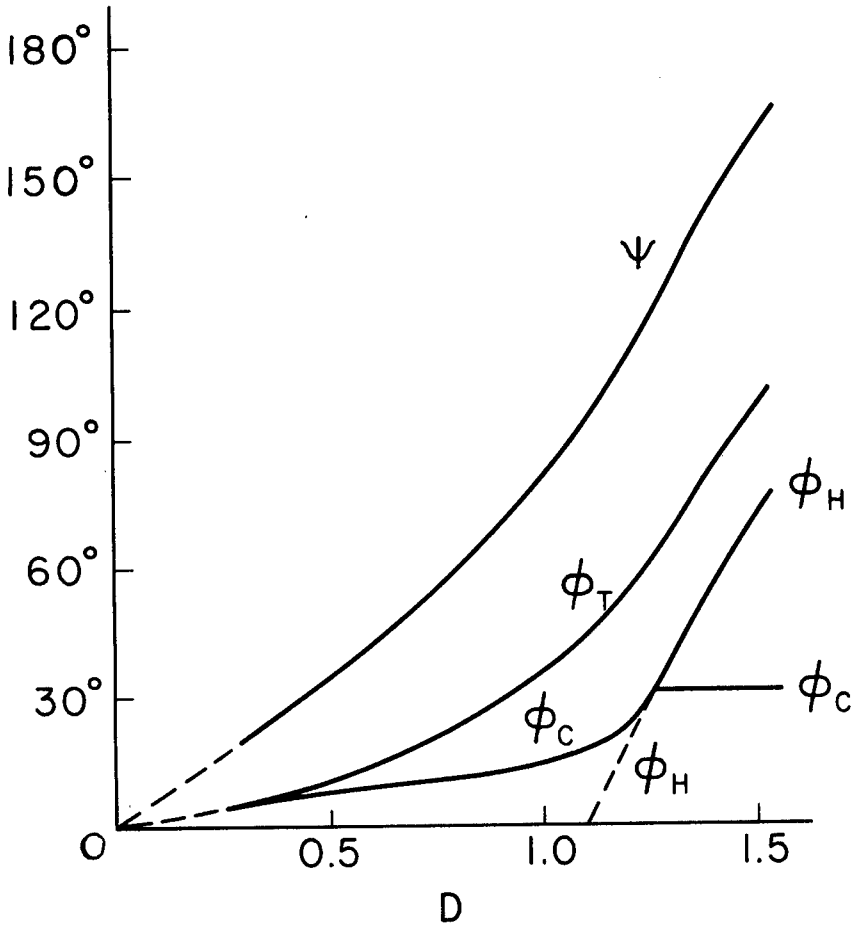

Fig. 9 Geometry dependence on dimensionless tube displacement D: t/R=.6, a/R = 1.75, ε_c = .02, and μ = 0.

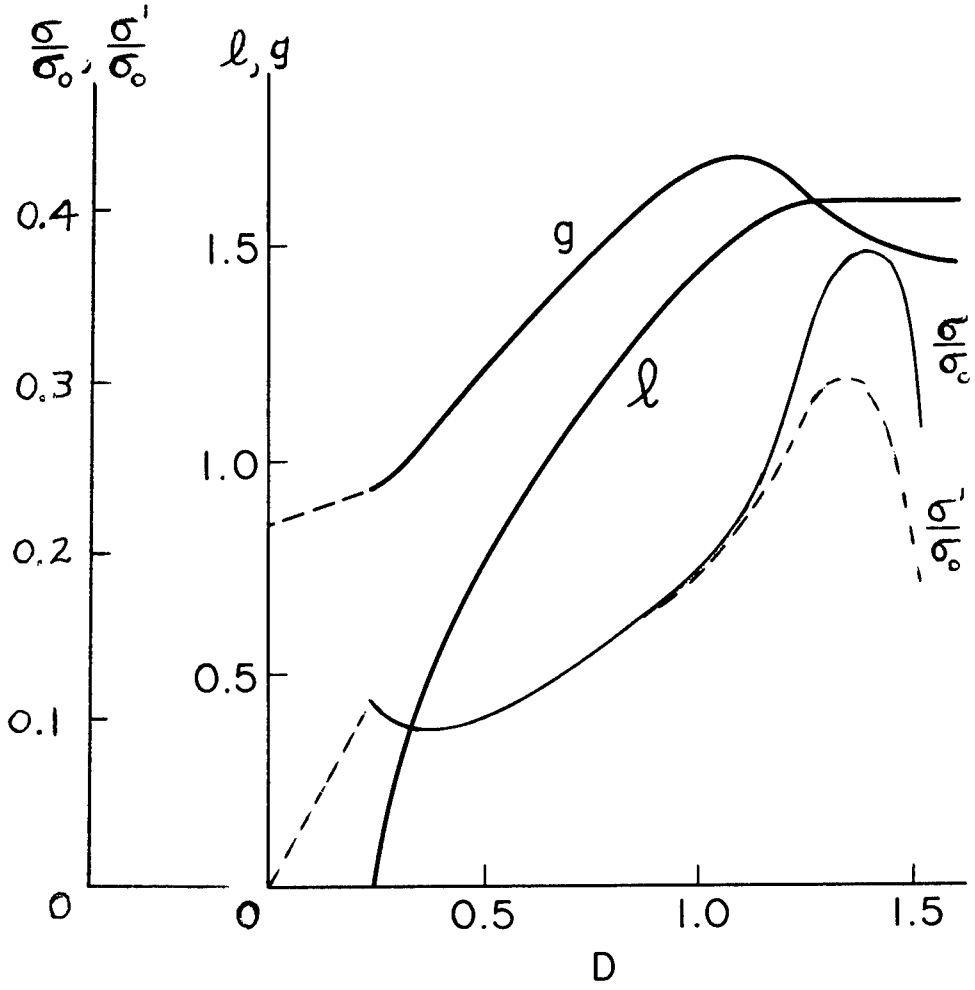

Fig. 10 Crack growth and hinge movement as functions of tube dimensionless displacement: $t/R = .6$, $a/R = 1.75$, $\varepsilon_c = .02$, and $\mu = 0$.

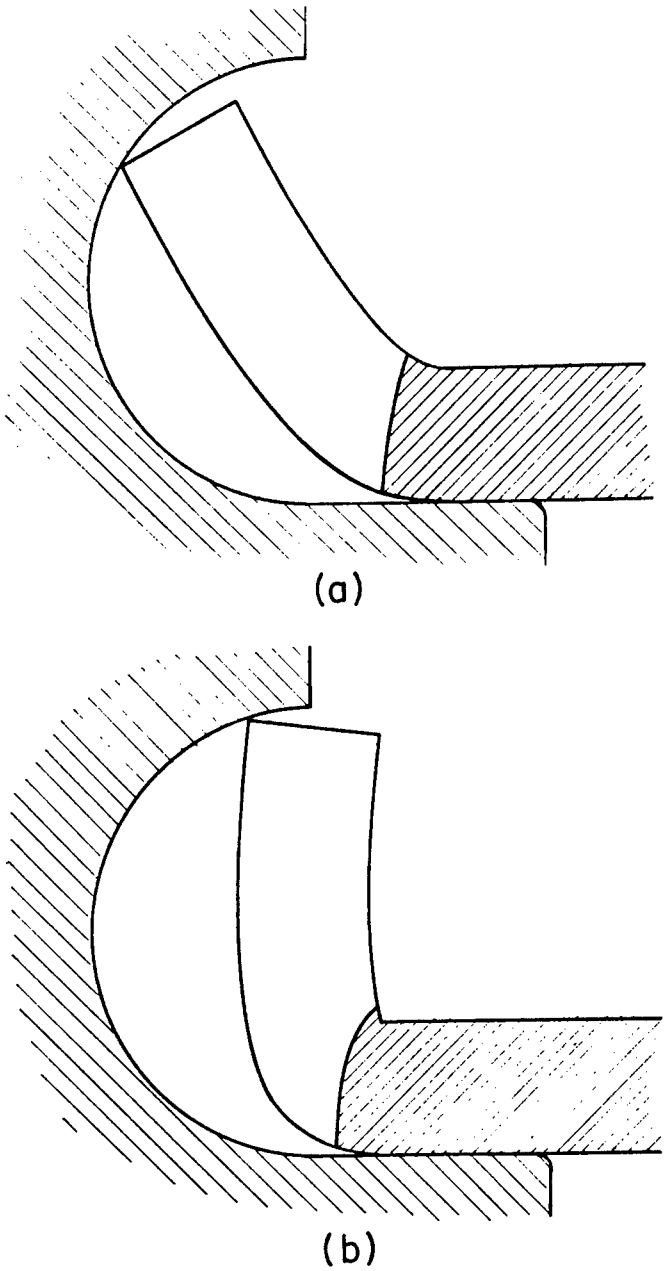

Fig. 11 Computed petal shapes: $t/R = .6$, $a/R = 1.75$, $\varepsilon_c = .02$, and $\mu = 0$. (a) When the cracks are arrested; (b) When the plastic hinges stop moving

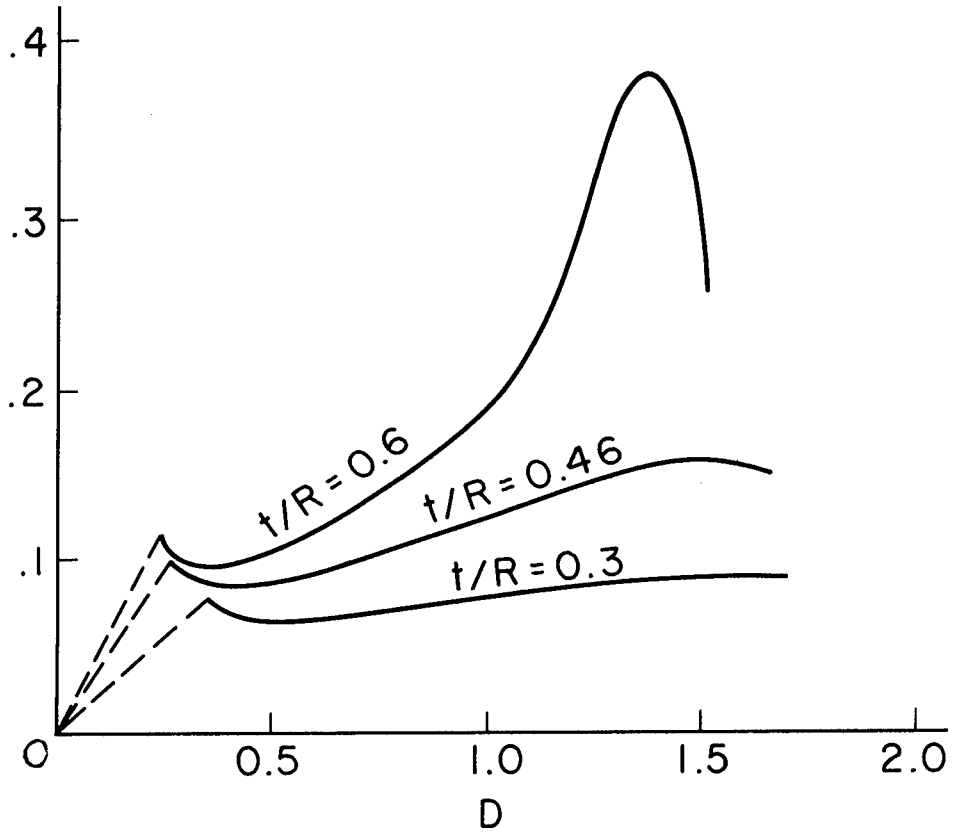

Fig. 12 Effect of t/R on the tube stress-displacement behavior: a/R = 1.75, ε_c = .02, and μ = 0

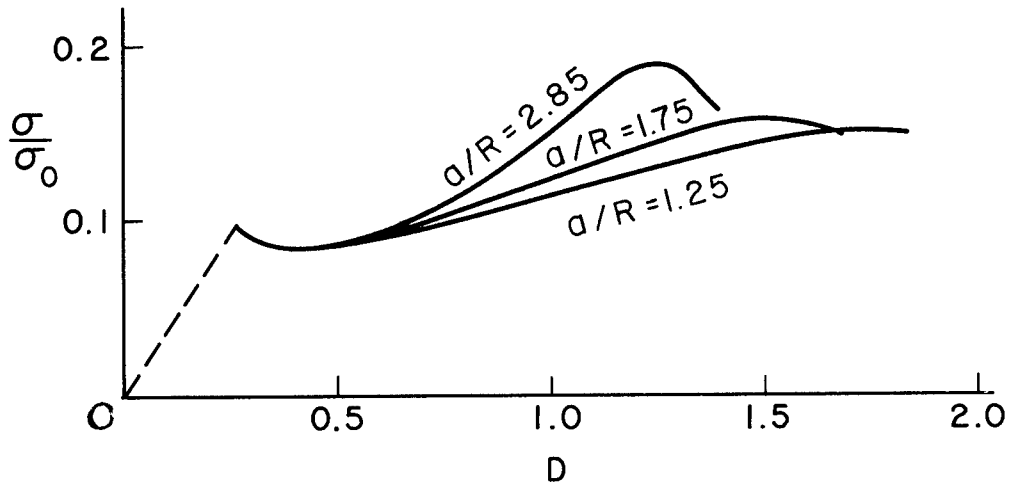

FIG. 13

Fig. 13 Effect of a/R on tube stress-tube displacement behavior: t/R = .46, ε_c = .02, and μ = 0

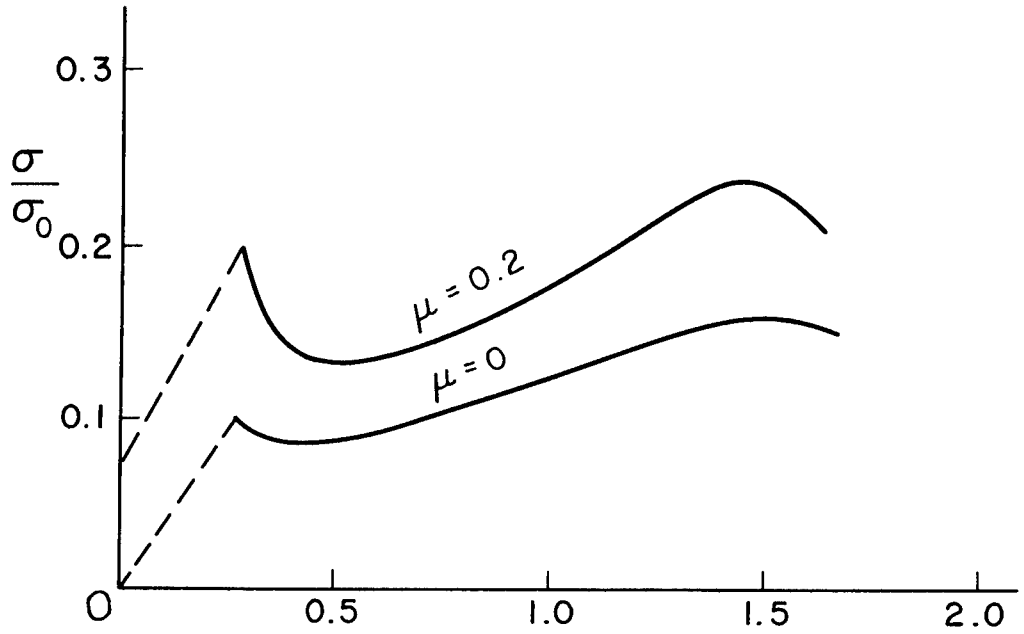

FIG. 14

Fig. 14 Effect of friction on tube stress-tube displacement behavior: t/R = .46, a/R = 1.75, and ε_c = .02

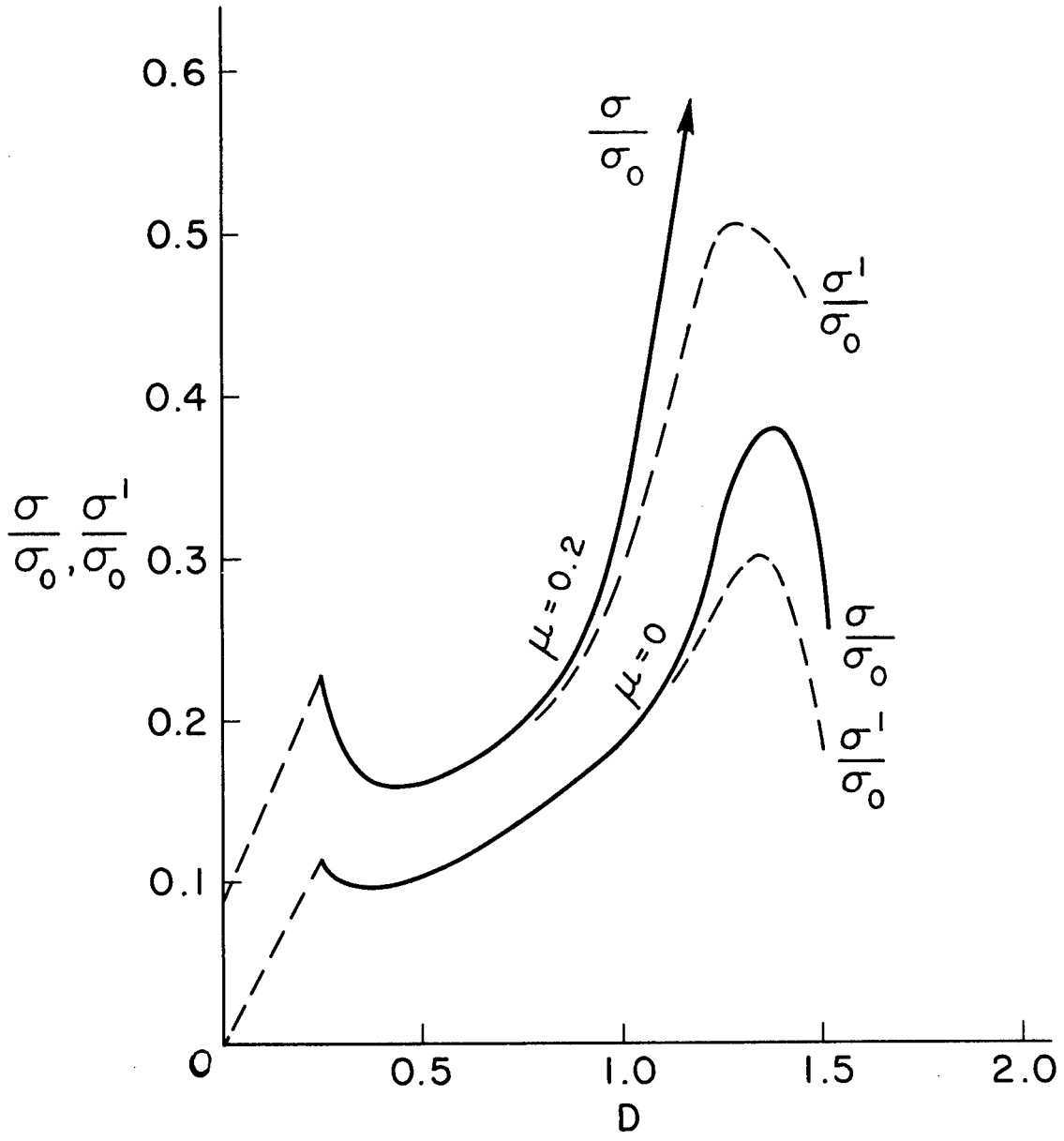

FIG. 15

Fig. 15 Effect of friction on tube stress-tube displacement behavior: $t/R = .6$, $a/R = 1.75$, and $\varepsilon_c = .02$.

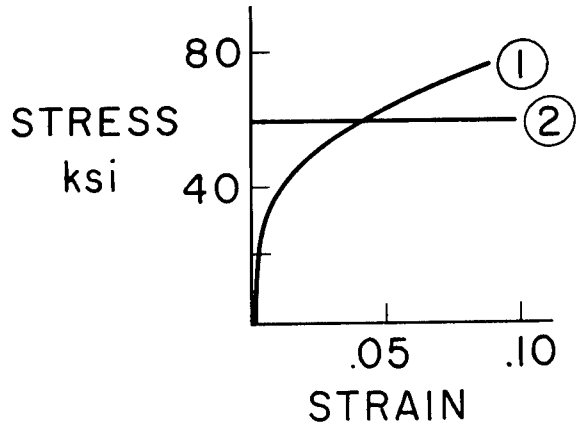

Fig. 16 Stress-strain curve for 2024 - T3 in compression and perfectly plastic idealization

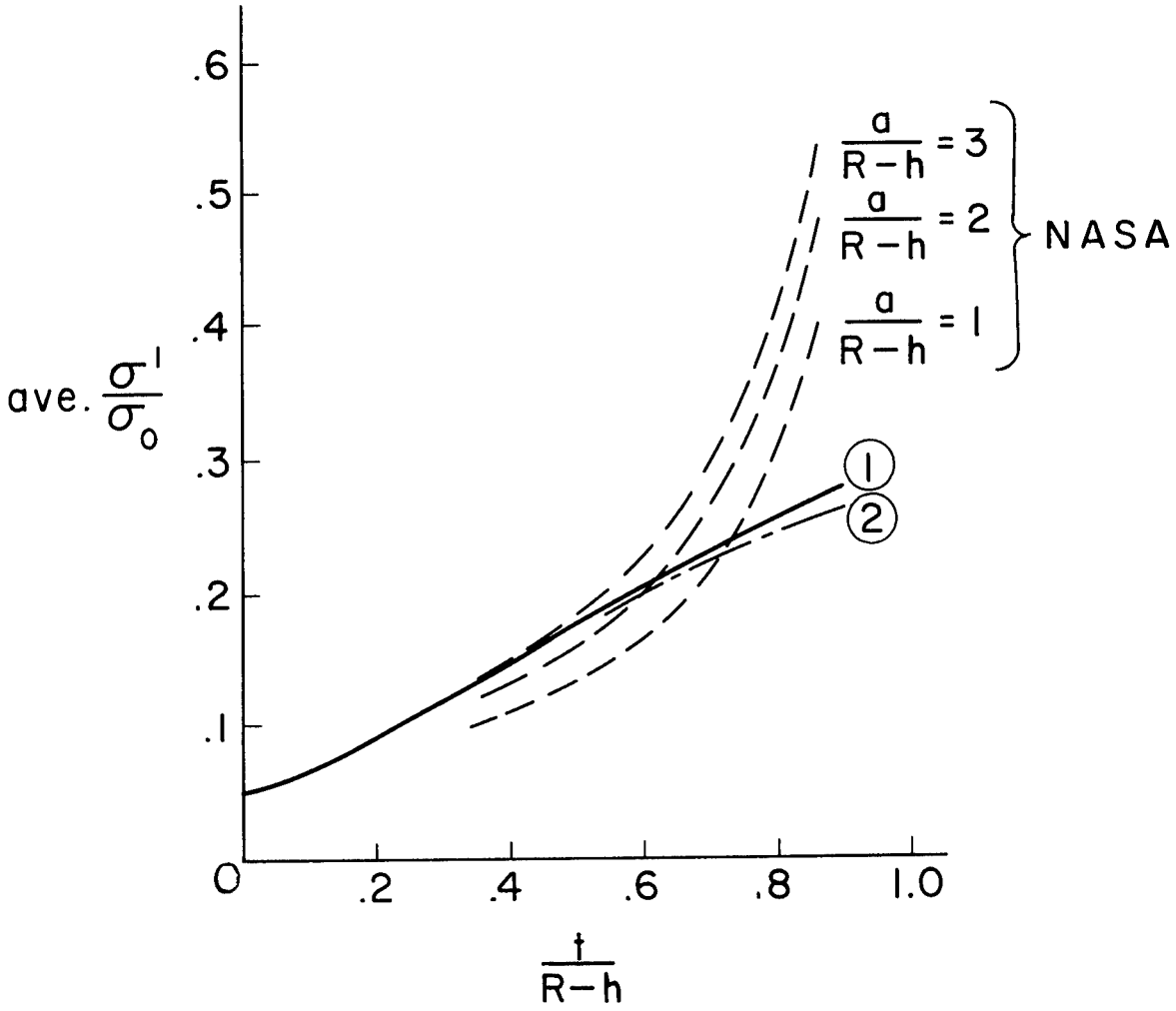

Fig. 17 Comparison of theoretical and test results

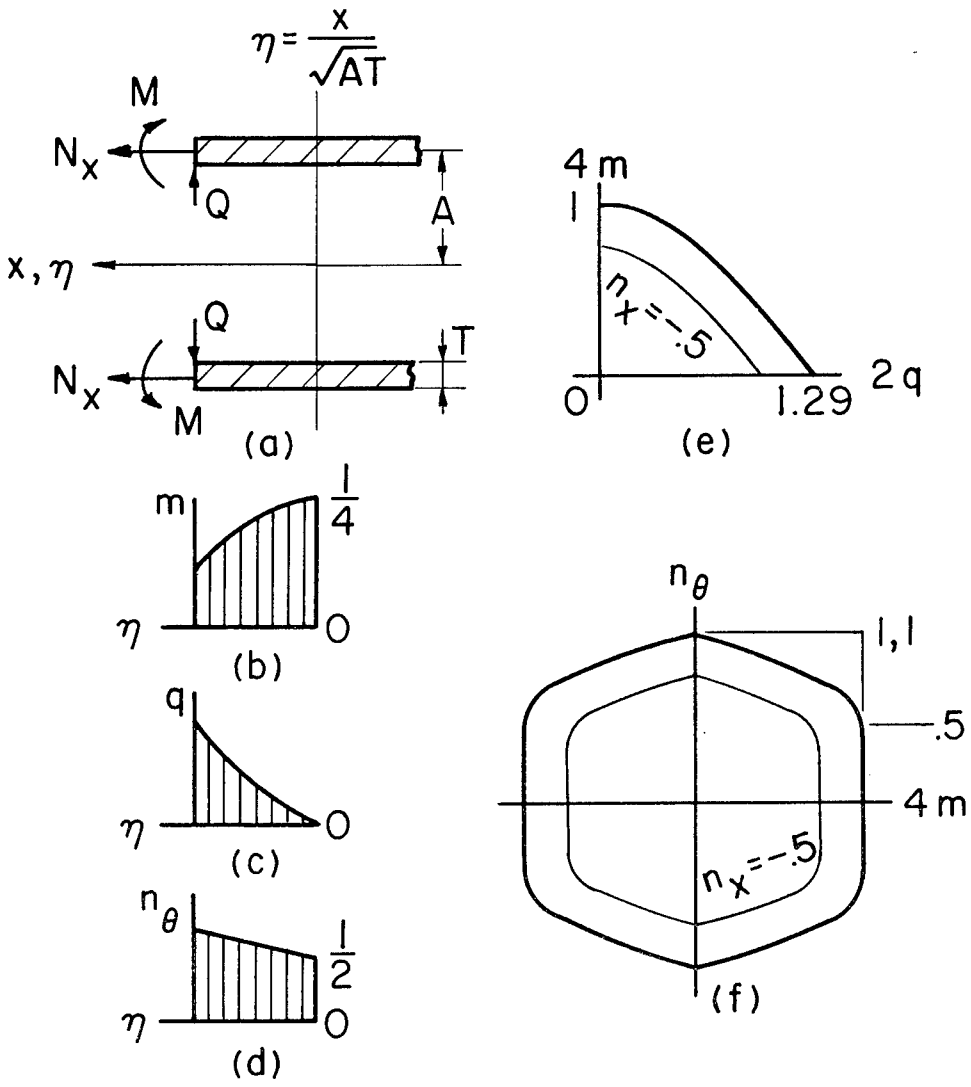

Fig. 18 (a) Shell and loading, (b) dimensionless bending moment, (c) dimensionless shearing force, (d) dimensionless circumferential tension, (e) yield condition in load space, (f) Tresca yield condition for a cylindrical shell.

"The aeronautical and space activities of the United States shall be conducted so as to contribute . . . to the expansion of human knowledge of phenomena in the atmosphere and space. The Administration shall provide for the widest practicable and appropriate dissemination of information concerning its activities and the results thereof."

—NATIONAL AERONAUTICS AND SPACE ACT OF 1958

NASA SCIENTIFIC AND TECHNICAL PUBLICATIONS

TECHNICAL REPORTS: Scientific and technical information considered important, complete, and a lasting contribution to existing knowledge.

TECHNICAL NOTES: Information less broad in scope but nevertheless of importance as a contribution to existing knowledge.

TECHNICAL MEMORANDUMS: Information receiving limited distribution because of preliminary data, security classification, or other reasons.

CONTRACTOR REPORTS: Technical information generated in connection with a NASA contract or grant and released under NASA auspices.

TECHNICAL TRANSLATIONS: Information published in a foreign language considered to merit NASA distribution in English.

TECHNICAL REPRINTS: Information derived from NASA activities and initially published in the form of journal articles.

SPECIAL PUBLICATIONS: Information derived from or of value to NASA activities but not necessarily reporting the results of individual NASA-programmed scientific efforts. Publications include conference proceedings, monographs, data compilations, handbooks, sourcebooks, and special bibliographies.

Details on the availability of these publications may be obtained from:

SCIENTIFIC AND TECHNICAL INFORMATION DIVISION

NATIONAL AERONAUTICS AND SPACE ADMINISTRATION

Washington, D.C. 20546